Electronic Supplementary Information (ESI) for

Screening Metal Cation Additives Driven by Differential Capacitance for Zn Batteries

Zhengqiang Hu,‡[a] Fengling Zhang,‡[a] Feng Wu,[abc] Huirong Wang,[a] Anbin Zhou,[a] Yi Chen,[a] Tianyang Xue,[a] Renjie Chen,[abc] Li Li*[abc]*

Experimental Section/Methods

Preparation of electrolyte: All sulfates (AR 99.7%) utilized in this experiment are purchased from Shanghai Aladdin Bio-Chem Technology Co., LTD. The ZS electrolyte was prepared by dissolving 5.751 g $ZnSO_4$ $7H_2O$ into 10 mL deionized (ID) water. The $ZnSO_4$ (ZS) electrolyte with different additives was acquired via adding 10 mmol sulfate into 10 mL of ZS electrolyte.

Preparation of cathode: The LMO powders were purchased from Canrd Technology Co. Ltd and used without further purification. The $Zn_3V_3O_8$ (ZVO) was fabricated by a hydrothermal method.[1] Firstly, 0.4 mmol commercial NH_4VO_3 (Aladdin AR) was dissolved in a mixture of 60 mL water and ethylene glycol at 80 °C (volume ratio 1:1) and stirred vigorously to form transparent solution. Then 0.4 mmol $Zn(NO_3)_2$ $6H_2O$ (Aladdin AR) was added to the above solution to obtain homogeneous yellow solution. The above mixture solution was transferred to 100 mL Teflon-lined autoclave and held at 200 °C for 30 h. After cooling down to room temperature, the synthesized products were collected by centrifugation, washed three times with ID water and ethanol, finally dried in vacuum at 60 °C for 12 h.

Electrochemical measurements: Electrochemical measurements were conducted using CR2032 coin-type cells. The cathodes, either LMO or ZVO, were prepared by mixing 80 wt% LMO or ZVO, 10 wt% Super P carbon (Canrd New Energy Technology Co. Ltd), and 10 wt% Polytetrafluoroethylene. The obtained slurry was coated on the Ti mesh and dried at 60 °C for 12 h under vacuum. The mass loading of active material on the Ti mesh was about 10-13 mg cm^{-2}. Glass fiber (GF-D Whatman) was used as the separator. Zn foils with a thickness of 100 µm as the electrode was employed for Zn-Ti or Zn-Cu cells. 1 M Li_2SO_4 was added into electrolyte for Zn-LMO cells. 50 µm Zn foil after polished was employed for high ZUR test. The mass loading is ~30 mg cm^{-2}, corresponding to theoretical capacities of ~25 mAh cm^{-2}. Galvanostatic charge and discharge (GCD) measurements were performed on a Neware battery systems instrument (CT-4008T) after a resting period of 2 hours. Cyclic voltammetry (CV), Linear Sweep Voltammetry (LSV), and Electrochemical Impedance Spectroscopy (EIS) tests were carried out using a CHI 660e electrochemical workstation (ChenHua Instruments Co.). The corrosion behavior was investigated using a three-electrode system, with Zn foil as the working electrode, Pt as the counter electrode, and Ag/AgCl as the reference electrode, on the CorrTest CS2350H electrochemical workstation (Wuhan CorrTest Instrument Corp., Ltd., China).

Materials characterization: The phase structure of materials was investigated using D8-X-ray diffraction (XRD, Bruker AXS, WI, USA). In situ XRD of Zn-Zn cell were employed 10 μm Zn foil. The interface morphologies of the Zn plating process were characterized using an optical microscope (Leica DVM6). Atomic force microscopy (AFM) images were collected using the Icon (Bruker) AFM. Attenuated Total Reflectance-Fourier Transform Infrared Spectroscopy (ATR-FTIR) spectra were obtained using the Bruker Alpha FT-IR spectrometer. In-situ (differential electrochemical mass spectrometry) DEMS was performed using a commercial mass spectrometer (Hiden HPR-40) with a Zn-Zn cell containing Zn electrodes, a glass fiber separator, and a stainless-steel spacer (height: 1 mm). Prior to testing, the system was purged with Ar for 12 hours (~5×10^6 Torr), and then the resulting gas was utilized during 5 mA cm^{-2} charging/discharging. In situ Raman analysis of Zn-Cu cells was conducted using the DXR Raman microscope with an excitation wavelength of 532 nm.

Molecular dynamics simulation: Molecular dynamics (MD) simulations were performed using GROMACS2018.8 package[2] and AMBER99SB-ILDN force field.[3] SO_4^{2-} , Zn metal and Ce^{4+} force-field parameters were generated by Sobtop[4], and the corresponding atom charges were based on restrained electrostatic potential 2 (RESP2) charges. The SPC/E water model was employed to simulate the properties of H_2O. The compositions of species for the MD simulations were provided in Table S4. Van der Waals (vdW) and electrostatic interactions were treated using the Cut-off and Particle-Mesh-Ewald (PME) method, respectively. A cutoff length of 10 Å was used in the calculation of electrostatic interactions and non-electrostatic interactions in real space Each system was initially equilibrated for 10 ns (5000000 steps, 2 fs per step). During equilibrium simulations, the Velocity-rescale thermostat and the Berendsen barostat were used to control the system temperature and pressure. The system was gradually annealed from 0 to 298 K over a duration of 0.5 ns, followed by a 5.0 ns equilibration period to reach a stable state. Temperature coupling was carried out using the V-rescale method, while pressure coupling utilized the Berendsen method. Subsequently, a 10 ns production simulation was conducted for post-processing analysis, during which the pressure coupling method was switched to Parrinello-Rahman to better capture the system's dynamic behavior. To calculate the radial distribution functions, a GROMACS built-in module was employed. Furthermore, the coordination number and snapshots (Fig. S4 and S5) of the MD simulation were generated using VMD software.[5]

Finite Element analysis Method: Zn electrodeposition was modelled and simulated using COMSOL Multiphysics 6.0. The simulation area had a height of 20 μm and a width of 50 μm. The Zn deposition process was described by the Butler-Volmer equation, which needed to account for the ion concentration on the surface due to Ce^{4+} adsorption in ZS-Na-L electrolyte. The Butler-Volmer equation is given as follows:[6, 7]

$$i_{loc} = -(C' - k\theta)\exp\left(\frac{-(\alpha - k'\theta)F\eta}{RT}\right)i_0 \quad (2)$$

Where: θ is the coverage of adsorbed inhibiting additive and cannot exceed unity. C' is the coefficient of Zn^{2+} concentration. k is the coefficient of Ce^{4+}. k' is the inhibiting transfer coefficient of Ce^{4+}. F is the Faraday constant. R is the molar gas constant. T is the ambient temperature. η is the overpotential. i_0 is the exchange current density. Before simulation, semi-ellipse nucleuses were set. (Note: The i_{loc} in the equation might represent the local current density at the surface). The mesh distribution of simulations model is shown in Fig. S13.

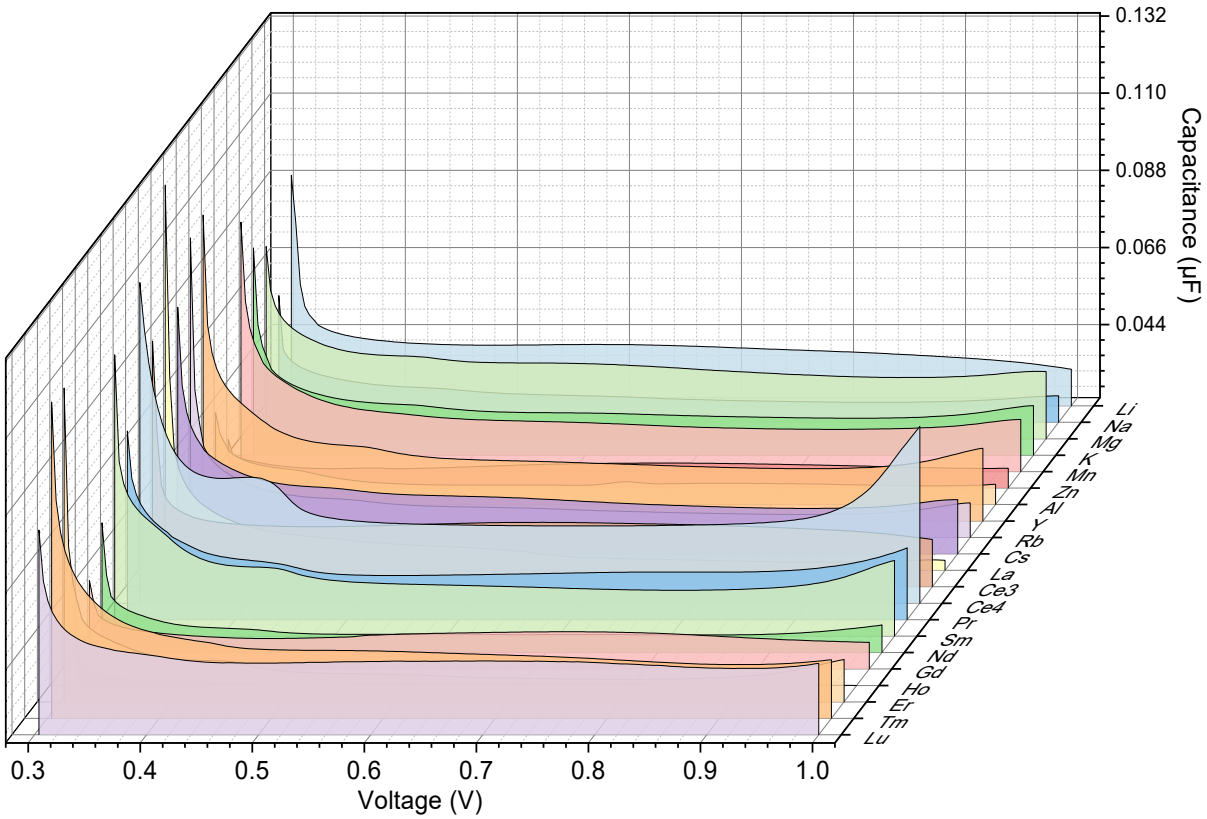

Fig. S1 The differential capacitance-potential curves in ZS electrolyte with different metal cations additive.

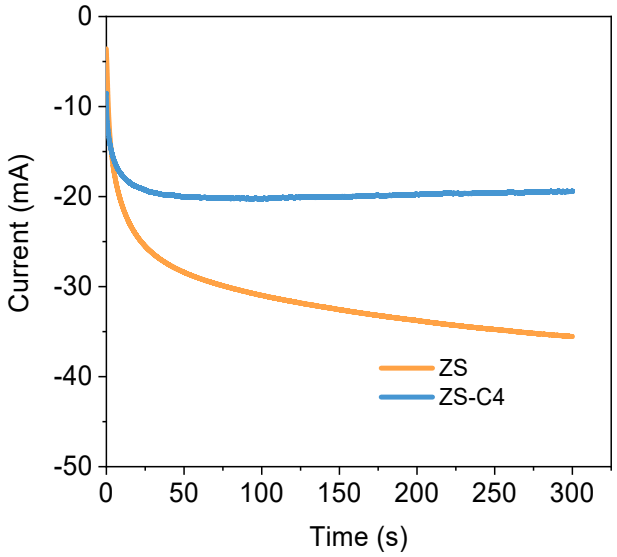

Fig. S2 Chronoamperogram (CA) of Zn-Zn cells at an overpotential of -150 mV.

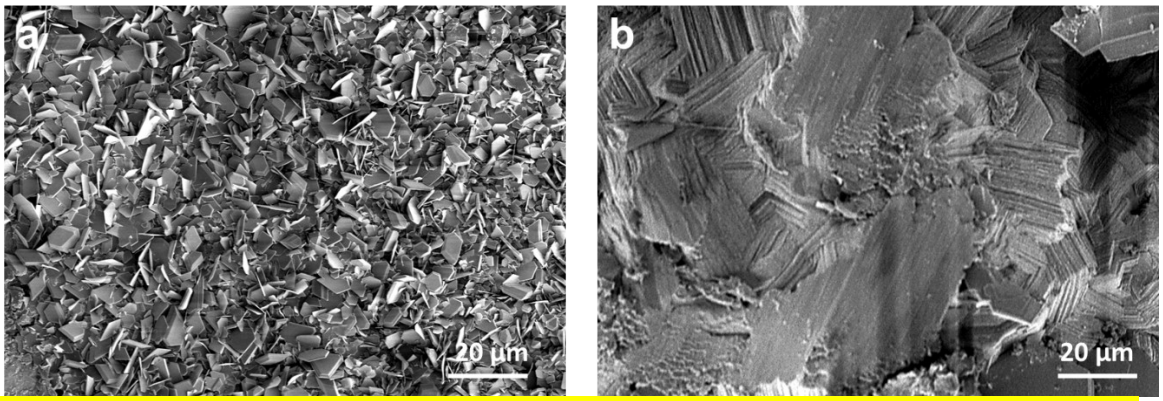

Fig. S3 The SEM images of cycled Zn anode in (a) ZS electrolyte and (b) ZS-C4 electrolyte.

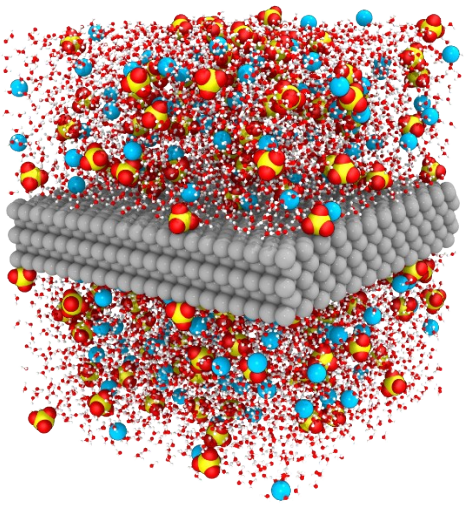

Fig. S4 The snapshots of 2 M $ZnSO_4$+ 25 mmol $Ce(SO_4)_2$.

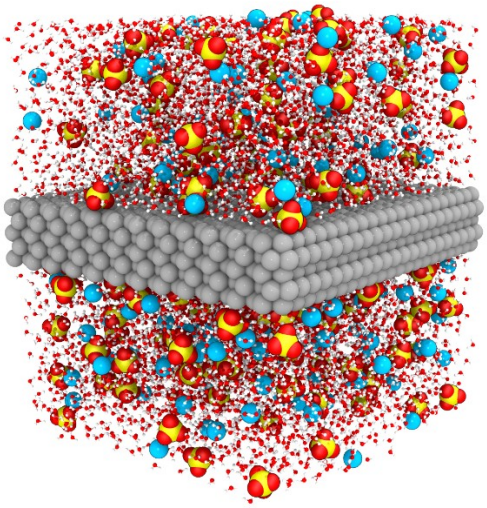

Fig. S5 The snapshots of ZS electrolyte.

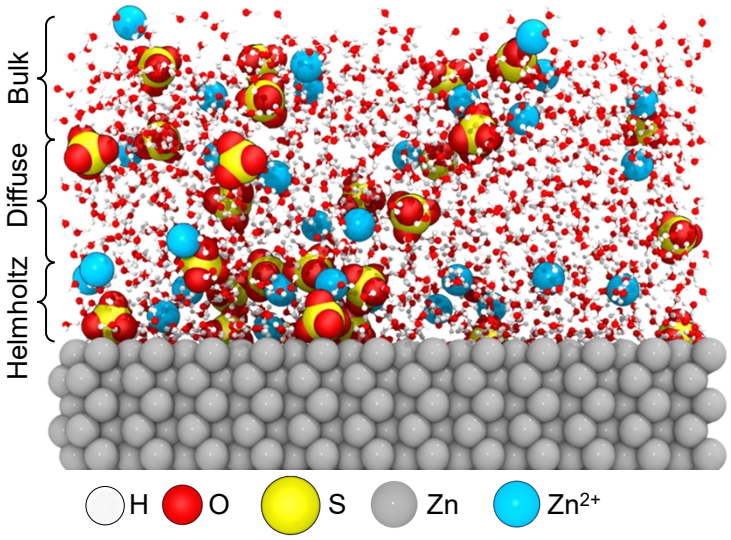

Fig. S6 The snapshot of EDL structure for Zn metal interface in ZS electrolyte.

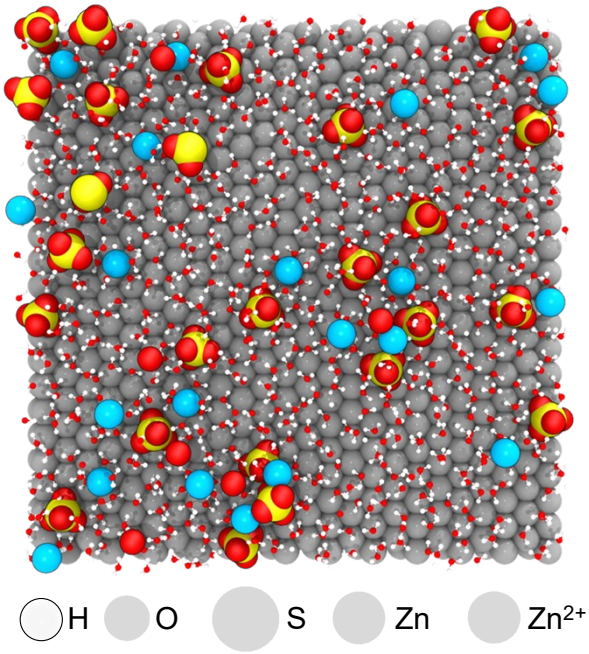

Fig. S7 The cross-sectional image of simulated Helmholtz region in ZS electrolyte.

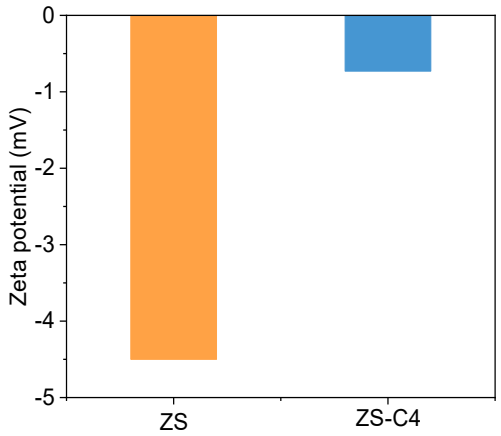

Fig. S8 Zeta potentials of Zn deposiitons in ZS and ZS-C4 electrolyte.

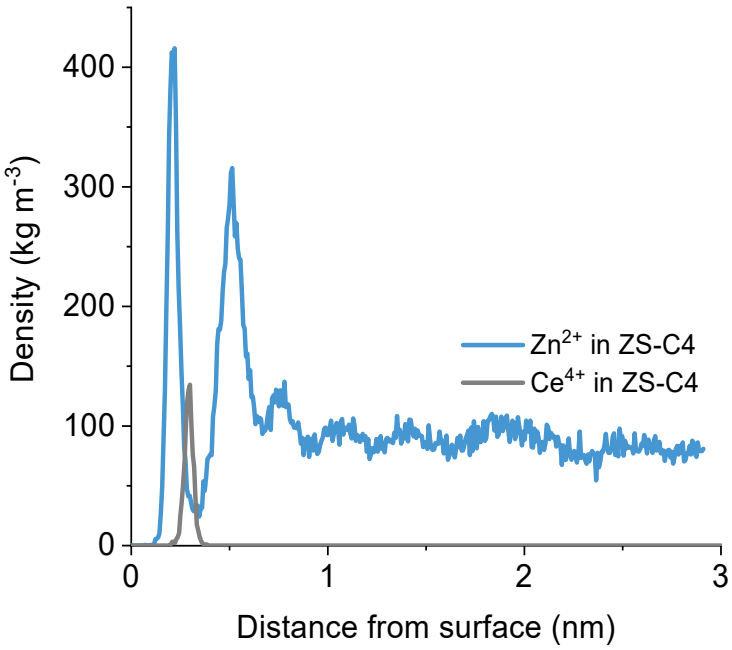

Fig. S9 The density profile of Ce^{4+} and Zn^{2+} near the Zn anode in ZS-C4 electrolyte.

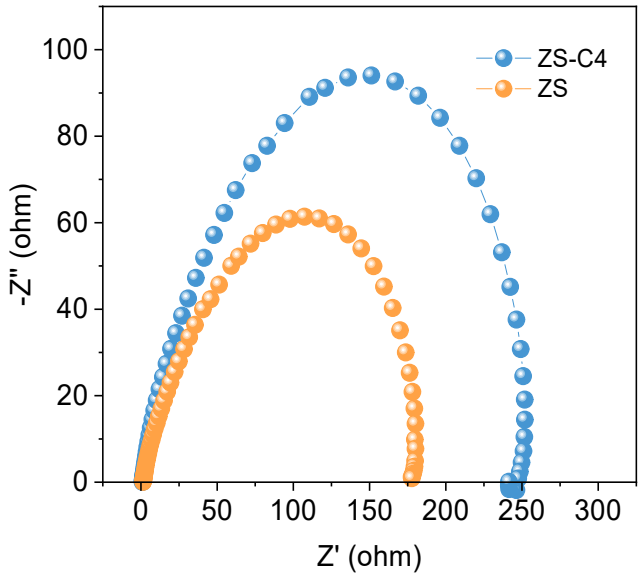

Fig. S10 EIS of the Zn-Zn cell in ZS and ZS-C4 electrolyte.

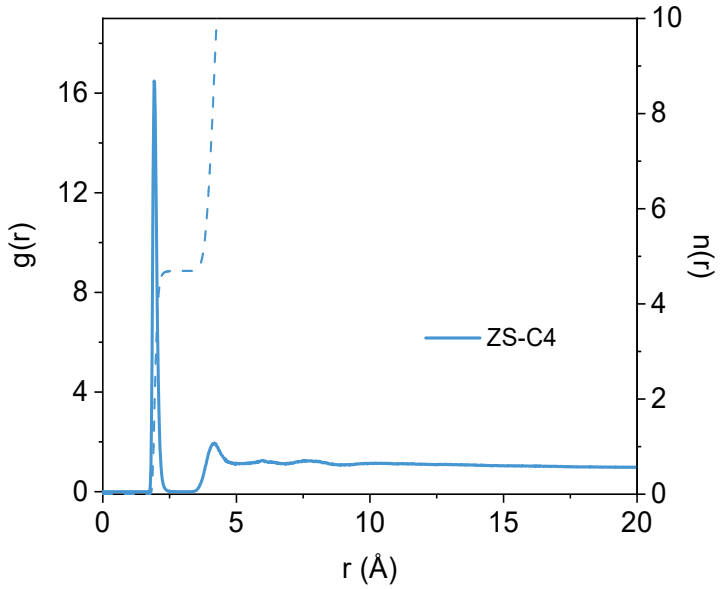

Fig. S11 RDF for Zn^{2+}-O (H_2O) collected from ZS-C4 electrolyte.

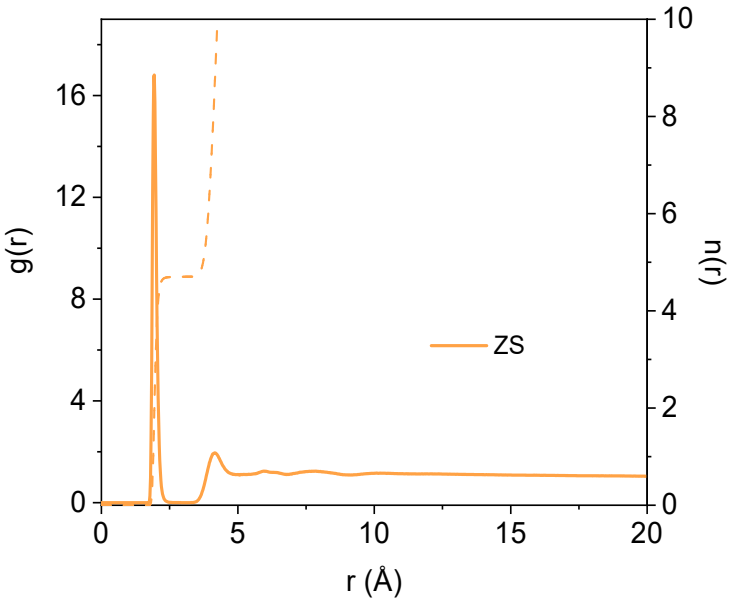

Fig. S12 RDF for Zn^{2+}-O (H_2O) collected from ZS electrolyte.

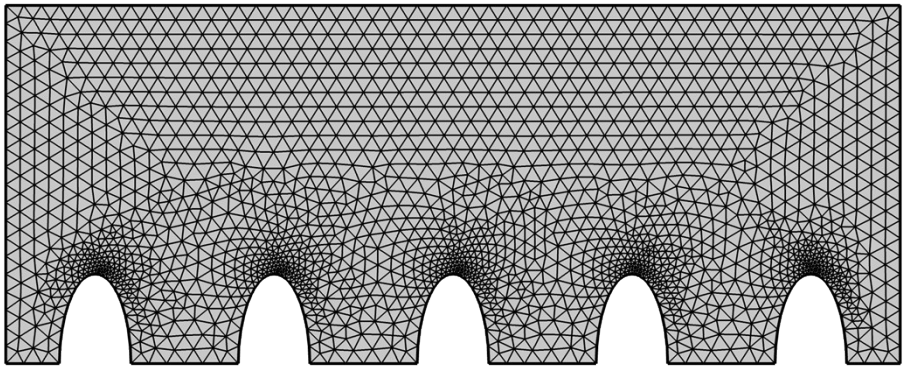

Fig. S13 Mesh distribution of finite element method simulations.

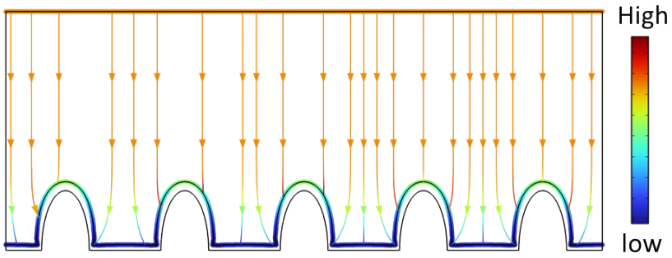

Fig. S14 The current distribution on electrode surface in ZS electrolyte.

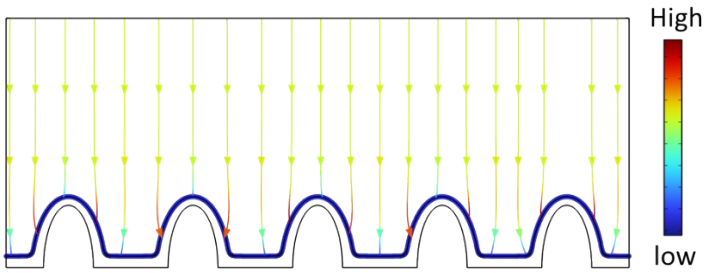

Fig. S15 The current distribution on electrode surface in ZS-C4 electrolyte.

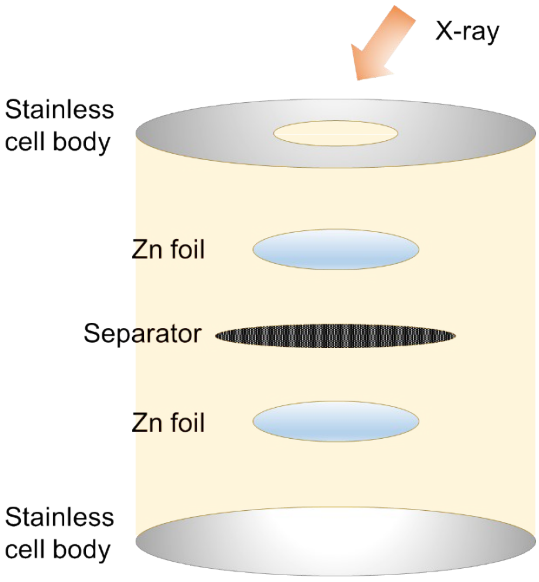

Fig. S16 In situ XRD mold for Zn-Zn cell.

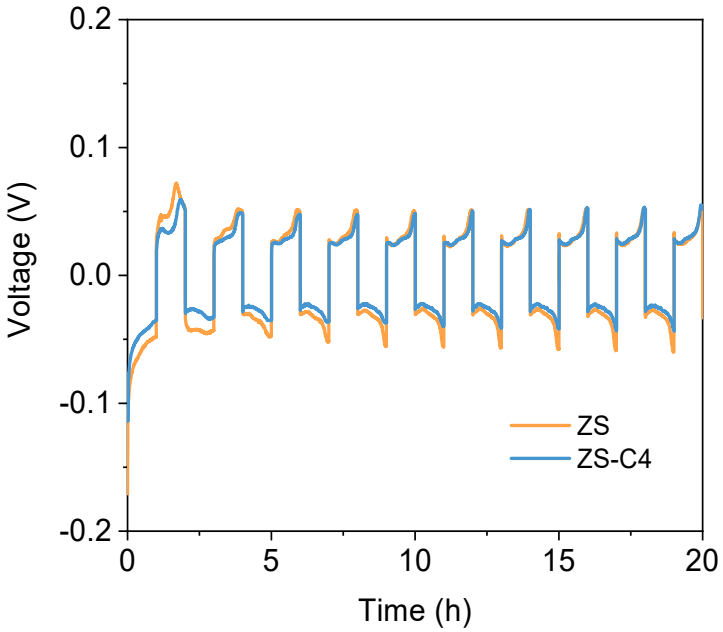

Fig. S17 Charging/discharging curves of Zn-Zn cells during in-situ XRD test under current density and capacities of 5 mA cm^{-2} and 5 mAh cm^{-2}.

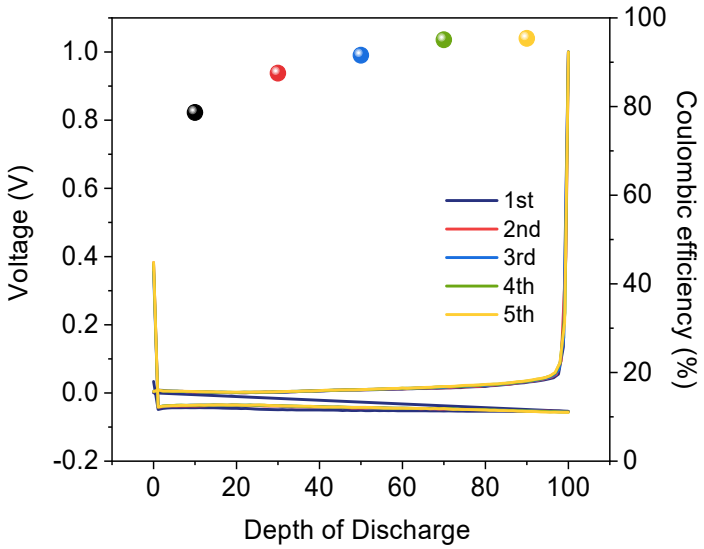

Fig. S18 The voltage profiles and coulombic efficiency in ZS electrolyte during in situ Raman test.

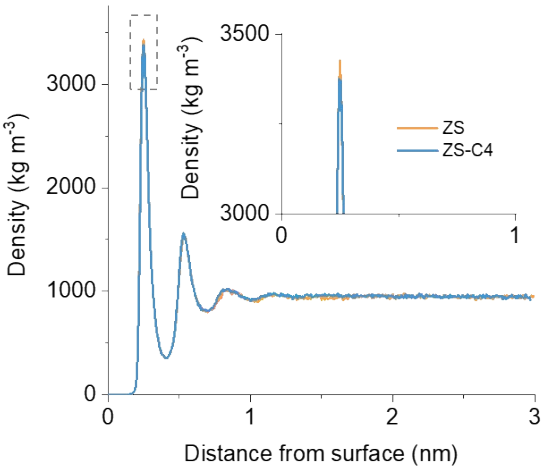

Fig. S19 Density profiles of water for Zn metal surfaces with/without Ce^{4+}.

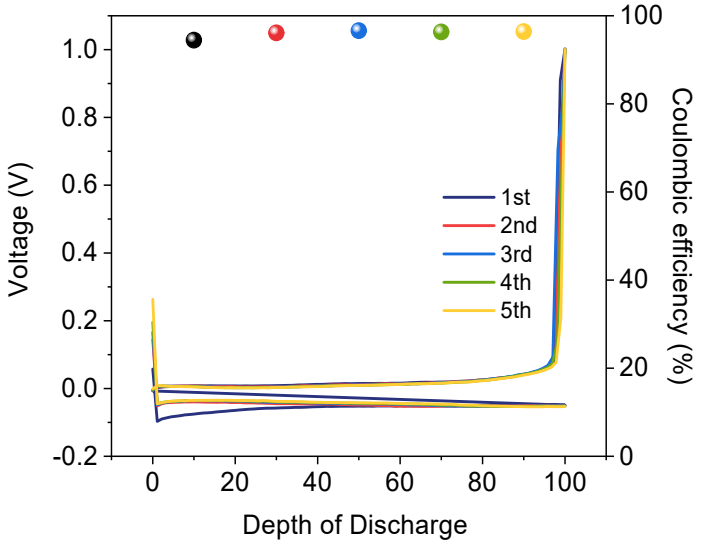

Fig. S20 The voltage profiles and coulombic efficiency in ZS-C4 electrolyte during in situ Raman test.

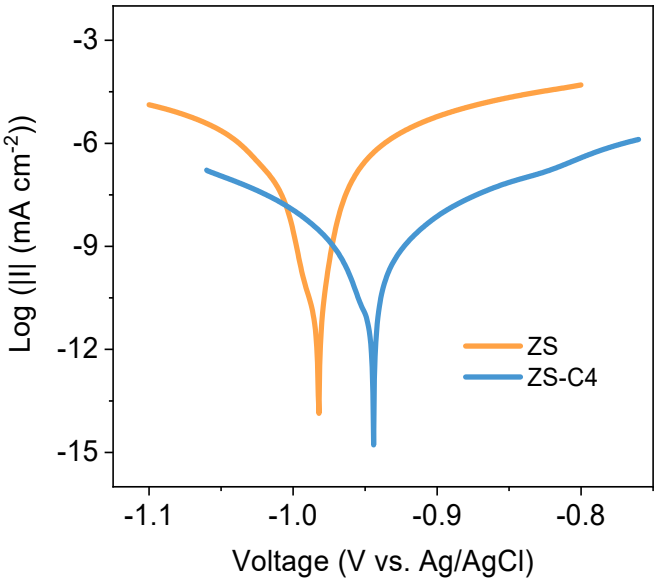

Fig. S21 Linear polarization curves of Zn electrodes in ZS and ZS-C4 electrolytes using three-electrode cell.

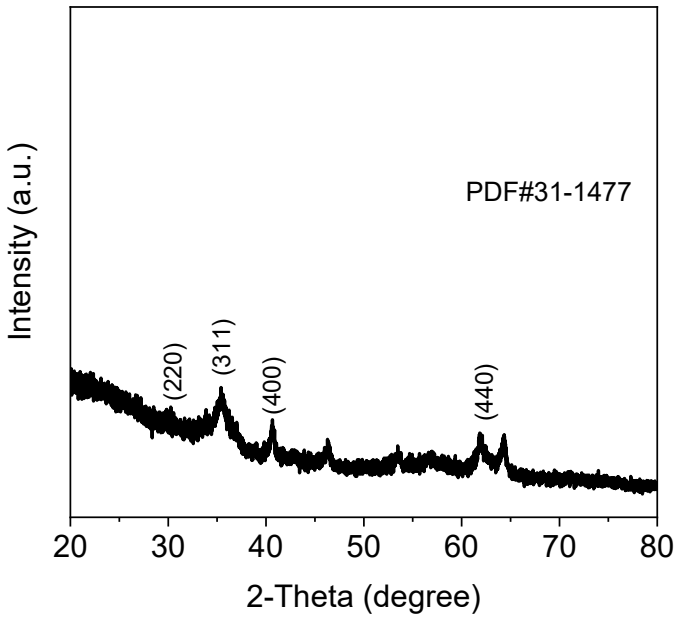

Fig. S22 XRD pattern of ZVO.

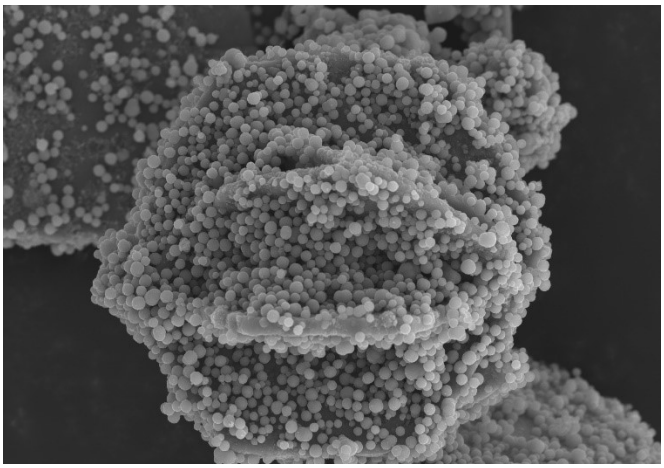

Fig. S23 SEM pattern of ZVO.

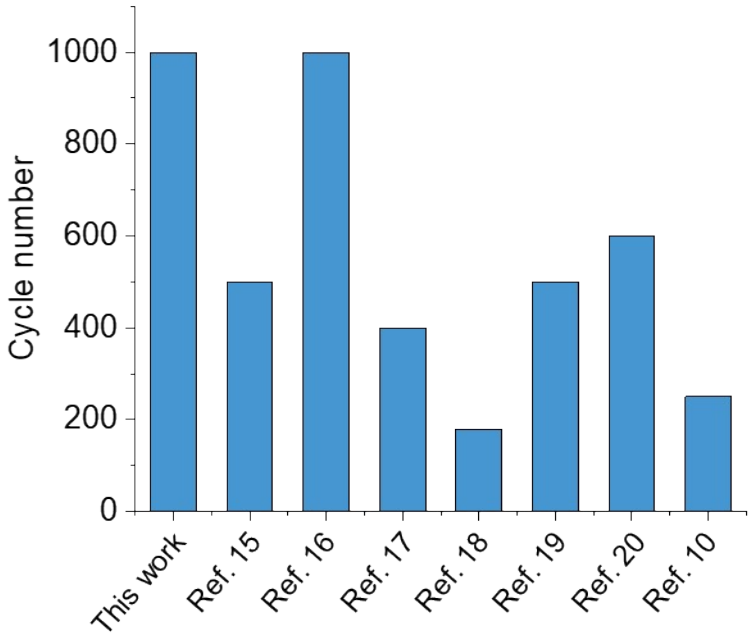

Fig. S24 Comparasion of cycle performance of this work with previous reports.

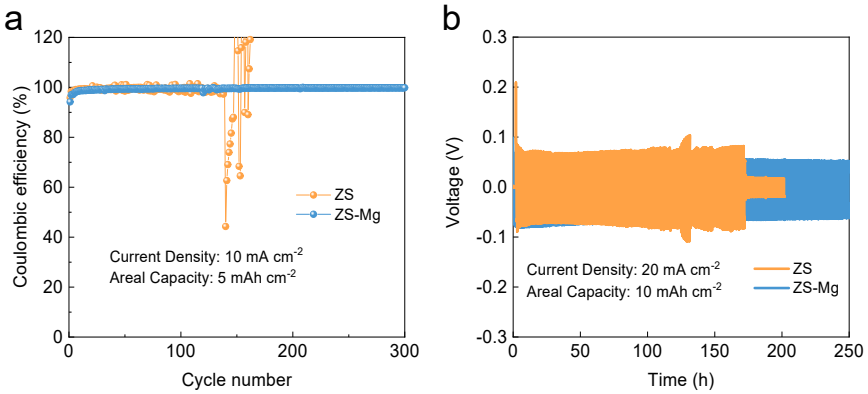

Fig. S25 Comparison of electrochemcial performance in ZS and ZS-Mg electrolyte (a) CE measurements of Zn-Cu cell under different electrolytes; (b) long-term galvanostatic Zn plating/stripping in Zn-Zn cells.

Table S1 Prices of different sulfates

Name	CAS Number	Valence state of metal cation	Price 10^4 \$ t^{-1}
Li_2SO_4	10377-48-7	+1	1.3
Na_2SO_4	7757-82-6	+1	1.3
$MgSO_4·H_2O$	14168-73-1	+2	1.3
$Al_2(SO_4)_3$	10043-01-3	+3	12.99
K_2SO_4	7778-80-5	+1	2.6
$MnSO_4$	7785-87-7	+2	3.9
$ZnSO_4·7H_2O$	7446-20-0	+2	25.97
Rb_2SO_4	7488-54-2	+1	298.7
$Y_2(SO_4)_3·8H_2O$	7446-33-5	+3	194.81
Cs_2SO_4	10294-54-9	+1	53.25
$La_2(SO_4)_3$	10099-60-2	+3	116.88
$Ce(SO_4)_2·8H_2O$	13590-82-84	+4	25.87
$Ce_2(SO_4)_3·8H_2O$	13454-94-9	+3	69.43
$Pr_2(SO_4)_3·8H_2O$	13510-41-3	+3	25.97
$Nd_2(SO_4)_3·8H_2O$	13477-91-3	+3	64.94
$Sm_2(SO_4)_3$	15123-65-6	+3	32.47
$Eu_2(SO_4)_3$	13537-15-0	+3	3350.65
$Gd_2(SO_4)_3·8H_2O$	13450-87-8	+3	207.79
$Tb_2(SO_4)_3$	13692-99-4	+3	2090.91
$Dy_2(SO_4)_3$	14373-91-2	+3	1688.31
$Ho_2(SO_4)_3·8H_2O$	15622-40-9	+3	740.26
$Er_2(SO_4)_3$	13478-49-4	+3	318.18
$Tm_2(SO_4)_3·8H_2O$	13778-40-0	+3	28
$Yb_2(SO_4)_3$	13469-97-1	+3	7623.38
$Lu_2(SO_4)_3·8H_2O$	1347-77-3	+3	29

The price is from Shanghai Aladdin Bio-Chem Technology Co., LTD.

Table S2 Comparison of electrochemical performance of this work with previously reported Zn-Zn cells.

Method	Current density mA cm^{-2}	Capacity mAh cm^{-2}	Ref.
Ce^{4+} additive	5	3.125	This work
Ce^{4+} additive	10	4	This work
Ce^{4+} additive	20	1.5	This work
α-CD	5	0.5	[8]
TCNQ	5	2.5	[9]
HPMA	20	0.14	[10]
L-cysteine	1	0.65	[11]
PZI	1	0.225	[12]
MXene	0.2	0.12	[13]
PAM@PPR	1	0.09	[14]

Table S3 Comparison of cycle life of this work with previously reported full cells.

Method	Cycle life	Ref.
Ce^{4+} additive	1000	This work
Bifunctional poly zwitterionic ionic liquid	500	[15]
Silk fibroin additive	1000	[16]
Small-Dipole-Molecule-Containing Electrolytes	400	[17]
N-Doped Graphene coating	180	[18]
Ammonium acetate additive	500	[19]
Copper mesh substrate	600	[20]
Hexamethylphosphoramide Additive	250	[10]

Table S4 the composition of the ion/molecules in electrolyte for MD simulations

Composition	H_2O	$ZnSO_4$	$Ce(SO_4)_2$	Zn (002)
ZS	5931	160	-	2520
ZS+C4	6023	160	2	2520

Reference

1. W. Liang, D. Rao, T. Chen, R. Tang, J. Li and H. Jin, *Angew. Chem., Int. Ed.*, 2022, **61**, e202207779.
2. H. J. C. Berendsen, D. van der Spoel and R. van Drunen, *Comput. Phys. Commun.*, 1995, **91**, 43-56.
3. Y. Duan, C. Wu, S. Chowdhury, M. C. Lee, G. Xiong, W. Zhang, R. Yang, P. Cieplak, R. Luo, T. Lee, J. Caldwell, J. Wang and P. Kollman, *J. Comput. Chem.*, 2003, **24**, 1999-2012.
4. T. Lu.
5. W. Humphrey, A. Dalke and K. Schulten, *J. Mol. Graph.*, 1996, **14**, 33-38.
6. P. Sun, L. Ma, W. Zhou, M. Qiu, Z. Wang, D. Chao and W. Mai, *Angew. Chem., Int. Ed.*, 2021, **60**, 18247-18255.
7. D. Josell, T. P. Moffat and D. Wheeler, *J. Electrochem. Soc.*, 2007, **154**, D208.
8. K. Zhao, G. Fan, J. Liu, F. Liu, J. Li, X. Zhou, Y. Ni, M. Yu, Y. M. Zhang, H. Su, Q. Liu and F. Cheng, *J. Am. Chem. Soc.*, 2022, **144**, 11129-11137.
9. P. Xiong, C. Lin, Y. Wei, J.-H. Kim, G. Jang, K. Dai, L. Zeng, S. Huang, S. J. Kwon, S.-Y. Lee and H. S. Park, *ACS Energy Lett.*, 2023, **8**, 2718-2727.
10. M. Kim, J. Lee, Y. Kim, Y. Park, H. Kim and J. W. Choi, *J. Am. Chem. Soc.*, 2023, **145**, 15776–15787.
11. D. Li, Y. Tang, S. Liang, B. Lu, G. Chen and J. Zhou, *Energy Environ. Sci.*, 2023, **16**, 3381-3390.
12. Y. Wang, Q. Li, H. Hong, S. Yang, R. Zhang, X. Wang, X. Jin, B. Xiong, S. Bai and C. Zhi, *Nat. Commun.*, 2023, **14**, 3890.
13. J. Zhou, Y. Mei, F. Wu, Y. Hao, W. Ma, L. Li, M. Xie and R. Chen, *Angew. Chem., Int. Ed.*, 2023, **62**, e202304454.
14. H. Xia, G. Xu, X. Cao, C. Miao, H. Zhang, P. Chen, Y. Zhou, W. Zhang and Z. Sun, *Adv. Mater.*, 2023, **35**, e2301996.
15. R. Chen, Q. Liu, L. Xu, X. Zuo, F. Liu, J. Zhang, X. Zhou and L. Mai, *ACS Energy Lett.*, 2022, **7**, 1719-1727.
16. J. Xu, W. Lv, W. Yang, Y. Jin, Q. Jin, B. Sun, Z. Zhang, T. Wang, L. Zheng, X. Shi, B. Sun and G. Wang, *ACS Nano*, 2022, **16**, 11392–11404.
17. Z. Huang, T. Wang, X. Li, H. Cui, G. Liang, Q. Yang, Z. Chen, A. Chen, Y. Guo, J. Fan and C. Zhi, *Adv. Mater.*, 2022, **34**, e2106180.
18. J. Zhou, M. Xie, F. Wu, Y. Mei, Y. Hao, R. Huang, G. Wei, A. Liu, L. Li and R. Chen, *Adv. Mater.*, 2021, **33**, e2101649.
19. D. Han, Z. Wang, H. Lu, H. Li, C. Cui, Z. Zhang, R. Sun, C. Geng, Q. Liang, X. Guo, Y. Mo, X. Zhi, F. Kang, Z. Weng and Q. H. Yang, *Adv. Energy Mater.*, 2022, **12**, 2102982.
20. Q. Zhang, J. Luan, L. Fu, S. Wu, Y. Tang, X. Ji and H. Wang, *Angew. Chem., Int. Ed.*, 2019, **58**, 15841-15847.